Indium Segregation and Enrichment in Coherent $In_xGa_{1-x}As/GaAs$ Quantum Dots

X. Z. Liao,[1] J. Zou,[1] D. J. H. Cockayne,[1] R. Leon,[2] and C. Lobo[3]
[1]*Australian Key Centre for Microscopy & Microanalysis, The University of Sydney, Sydney NSW 2006, Australia*
[2]*Jet Propulsion Laboratory, California Institute of Technology, 4800 Oak Grove Drive, Pasadena, California 91109-8099*
[3]*Department of Electronic Materials Engineering, The Australian National University, Canberra ACT 0200, Australia*
(Received 17 November 1998)

Significant differences in the image features of $In_xGa_{1-x}As$ quantum dots (QDs) grown on (001) and vicinal (001) GaAs were seen in [001] on-zone bright-field transmission electron microscope images. Simulated images were obtained by modeling the strain field distribution of the QDs with finite element analysis and then using this model in dynamical electron diffraction contrast simulations. Comparison of the experimental images and the simulated images shows that (i) In segregation exists in the QDs and (ii) the average In content of the QDs is higher than the average In content of the film. [S0031-9007(99)09460-0]

PACS numbers: 81.05.Ea, 61.14.Lj, 61.16.Bg, 68.35.Dv

The composition, shape, and size of quantum dots (QDs) are essential parameters in determining their optoelectronic properties [1]. Many techniques have been used to study these parameters [2,3]. Among them, transmission electron microscopy (TEM) has been one of the most frequently used. It is well known that, under the usual dynamical two-beam or on-zone axis multibeam imaging conditions, the TEM diffraction contrast image arises largely from the strain field, which is sensitive to the composition, shape, size, and elastic constants of both the substrate and the QD. Consequently, it should be possible to obtain information about the composition, shape, and size of QDs from such images. However, to correctly interpret diffraction contrast images, image simulations are essential [2].

Obtaining the strain field distribution within and around the QDs is necessary for image simulations. Finite element analysis (FEA) methods have been widely and successfully used to study the strain field of nanometer-size semiconductor QDs and applied to TEM investigations. For example, Christiansen *et al.* [4] used FEA to obtain the displacement field of Ge(Si) islands grown on Si. Using convergent beam electron diffraction, their study showed that the displacement field obtained in this way is correct. Rosenauer *et al.* [3] determined the composition profile of $In_xGa_{1-x}As$ QDs using high resolution TEM and FEA. Benabbas *et al.* [5] applied FEA to generate strain fields of InAs/GaAs QDs, and they calculated two-beam dynamical electron diffraction contrast images to study their shape.

In this study, we use three dimensional anisotropic FEA to generate strain field distributions of $In_xGa_{1-x}As$ QDs grown on (001) GaAs. We then use these strain field distributions in multibeam dynamical electron diffraction calculations to produce contrast simulations of [001] on-zone bright-field TEM images. An earlier study [6] showed that the [001] on-zone bright-field imaging can be used to estimate the size of the unburied QDs. Here, we show that indium composition plays a role in defining the boundary of the TEM image and in determining several of the image features. Both electron diffraction patterns and comparison of the simulated and experimental images show that the composition of the dots is different from the composition of the thin film alloy from which the QDs formed. Our results also show significant indium redistribution within the QDs.

The observation of indium enrichment in $In_xGa_{1-x}As$ QDs has implications for the energy eigenvalues expected from these structures, and some of the earlier experimental results might need reconsideration in light of these findings. Similarly, the observation of indium redistribution implies an even more asymmetric confining potential than has been assumed, because of both strain and composition gradients within the QD structure.

Two samples of unburied nanometer-size $In_xGa_{1-x}As$ QDs were grown simultaneously by metal-organic chemical vapor deposition on a GaAs (001) (sample *A*) and vicinal (001) substrate [2° miscut towards (110)] (sample *B*) at the temperature of 590 °C. Details of sample preparation are described elsewhere [7]. Elemental analysis of the film using Rutherford backscattering spectrometry and low temperature photoluminescence spectroscopy of thick relaxed films indicates that the ternary composition of the film is $In_{0.6}Ga_{0.4}As$, corresponding to a lattice mismatch of 4.3% with the GaAs substrate.

TEM observation shows two distinct types of island in each of the two samples: small coherent islands (QDs) and a small concentration of larger, relaxed incoherent islands [8]. Consequently, assuming Vegard's law (lattice parameter is proportional to composition), their average composition was determined by measuring their lattice parameter from selected area diffraction patterns (SADPs) including the substrate and the relaxed islands, and using the diffraction spots of the substrate as the reference. Figures 1(a) and 1(b) show SADPs for sample *A* and sample *B*, respectively. These give lattice mismatches of

 0031-9007/99/82(25)/5148(4)$15.00

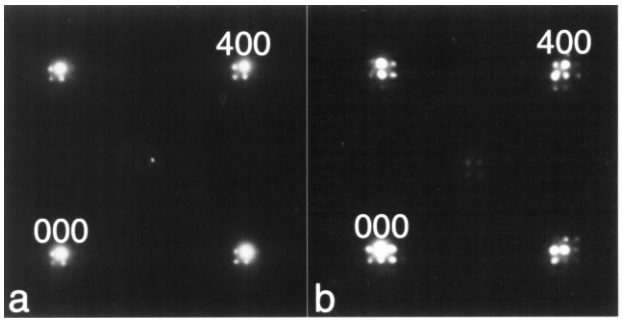

FIG. 1. [001] selected area electron diffraction patterns of large relaxed islands and the substrates taken from (a) samples *A* and (b) sample *B*.

5.7% ± 0.5% (sample *A*) and 6.2% ± 0.5% (sample *B*). Both of these values are significantly higher than the value of 4.3% corresponding to a composition $In_{0.6}Ga_{0.4}As$. This result is in agreement with the theoretical work of Tersoff [9], who, on the basis of free energy considerations, predicted segregation of the larger-misfit component (indium in our case) to the islands.

Figures 2(a) and 2(b) show experimental [001] on-zone bright-field images of coherent QDs in samples *A* and *B*, respectively. In Fig. 2(a), the images of the QDs have clear circular-shaped boundaries, with some images being slightly elliptical, and with a dark cross of triangular bars parallel to ⟨100⟩ within the boundaries. In Fig. 2(b), the image of each QD has two crosses; one cross is wider, with bars parallel to ⟨100⟩, while the other is narrower, with bars parallel to ⟨110⟩. Three questions arise: (i) What is the relationship between the circular-shaped boundary and the real QD edge, (ii) why is the diffraction contrast in the two images different, and (iii) does this difference provide information about the QDs?

A previous study [6,8] has shown that these QDs are lens shaped. In the model used in the finite element analysis of this paper, a spherical-cap-shaped dot is employed for simplicity. Figure 3, which also includes information about the displacement distribution (see discussion later), shows such a model in cross section, in which the fine lines are the finite element mesh used in the calculation. In this model, the half width of the dot (OA) (called the base radius) has been set equal to $4R/5$ (R is the radius of the sphere) and the height (OB) has been set equal to $2R/5$, so that the height-to-base diameter ratio is 1:4 to match the experimentally determined value [2,6].

The finite element calculation was performed using STRAND6 software [10]. Three dimensional models were generated by rotating the two dimensional section (shown in Fig. 3) 90° around [001]. The geometry is meshed with eight-node elements in most of the model, and with six-node triangular elements at areas connected to the rotation axis, to the edge A, and to the dot surface. Because the model has axial symmetry around [001], and because the crystal lattice of the sample has fourfold

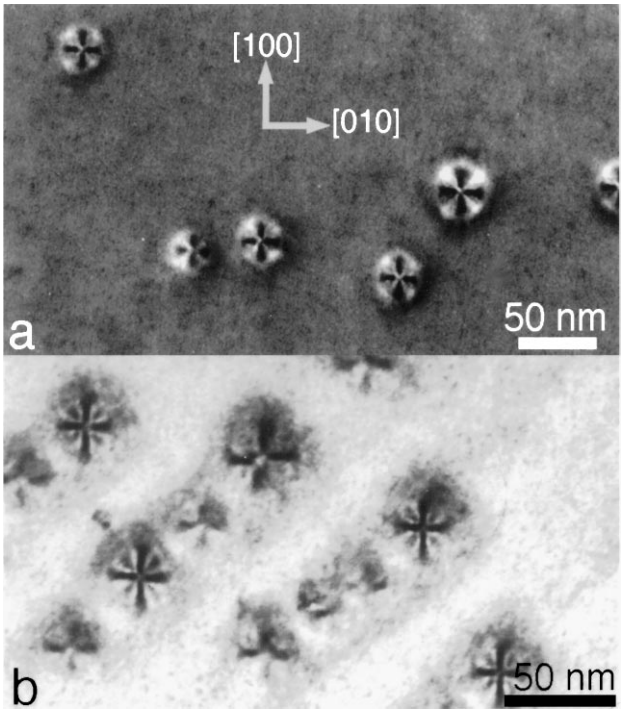

FIG. 2. [001] on-zone axis bright-field TEM images of $In_xGa_{1-x}As/GaAs$ coherent QDs in (a) sample *A* and (b) sample *B*.

symmetry, only one-quarter of the model needs to be calculated. Boundary conditions are set by the fourfold symmetry of the strain field, and by assuming that QDs are periodically arrayed in [100] and [010] directions. The lattice mismatch (f) between the $In_xGa_{1-x}As$ QDs and the GaAs substrate is represented by assuming the thermal expansion coefficients are $f(K^{-1})$ for the QDs and 0 (K^{-1}) for the substrate, and then by raising the

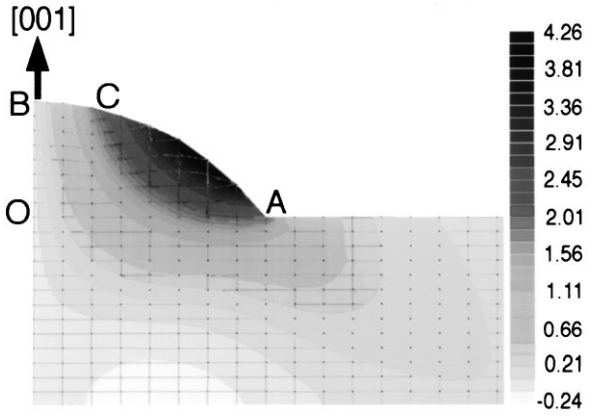

FIG. 3. The model of the (100) cross section of a spherical-cap-shaped QD. Only half of the model is shown as it is symmetrical about the axis OB. The distribution of the displacement U_{xy} (in Ångstroms) on this plane obtained by finite element analysis is shown. Values of the displacements are represented using different gray scales. The following geometrical parameters for the QD were used: base diameter, 40 nm; lattice mismatch, 4%.

temperature by 1 K. In the calculation, the anisotropic elastic constants of GaAs [11] were used for both the $In_xGa_{1-x}As$ QDs and the GaAs substrate.

The calculations show that the displacement field has axial symmetry inside the QD and fourfold symmetry outside the QD. The only component of the displacement field which contributes to the diffraction contrast of [001] on-zone bright-field images is the (001) plane component U_{xy} (ignoring upper layer line effects). A cross sectional distribution of U_{xy} for the (100) plane which passes through the center of the QD is also shown in Fig. 3. It is seen that U_{xy} is relatively small outside the QD (both below and beside the QD). For example, at a depth of approximately 0.6 of the QD height into the substrate, the maximum value of U_{xy} is less than 10% of the largest U_{xy} value within the QD, and the greatest U_{xy} values occur around the free surface region of the QD (between A and C in Fig. 3).

TEM image simulations were carried out using multibeam dynamical electron scattering theory [12] with the column approximation, and the absorption was considered using the perturbation method and by assuming the imaginary parts of Fourier coefficient of lattice potential to be one-tenth of their real counterparts [12]. Calculations with different values showed no significant differences to the images, except changes in relative contrast. For simplification, the structure factors of $In_xGa_{1-x}As$ and GaAs were assumed to be equal. The simulation area of $2d \times 2d$ (where d is the diameter of the dot) was divided into 32×32 columns. Because of this, the simulated images (Fig. 4) show some granularity.

Figures 4(a)–4(c) show simulated images for QDs with a base diameter of 40 nm and an aspect ratio of height to base diameter of 1:4, and for lattice mismatch values f from 4% to 7%. For $f = 4\%$ [Fig. 4(a)], the image has a circular dot boundary, a central cross with bars of constant width parallel to ⟨100⟩, and a bright spot at the center. Analysis shows that the circular boundary corresponds to the outer radius of the sphere used in the simulation. From Figs. 4(a)–4(c), it is noted that, with increasing lattice mismatch, (i) the bar widths of the cross become narrower, (ii) the center spot becomes smaller, and (iii) a second cross with bars parallel to ⟨110⟩ appears and becomes increasingly clear. Simultaneously, the image boundary becomes a little larger [up to 11% larger than the real size in the case of Fig. 4(c)] and blurred, and it loses its circular symmetry and gains fourfold symmetry. This change in symmetry can be explained by the strain field outside the QDs increasing as the mismatch increases, and the fourfold symmetry outside the dot is reflected in the image. Extensive image simulations show that the above image features remain unchanged when the thickness of the TEM specimen is greater than 40 nm.

Comparing the simulated images with the experimental ones, agreement is seen between Fig. 4(a) ($f = 4\%$) and Fig. 2(a) (sample *A*), and between Figs. 4(b) and 4(c) ($f = 6\%$ and 7%, respectively) and Fig. 2(b) (sample *B*). This is qualitatively in agreement with the diffraction patterns from the incoherent islands of sample *A* which give a mismatch of $5.7 \pm 0.5\%$ compared with $6.2 \pm 0.5\%$ of sample *B* (see above). These results suggest that both the incoherent islands and the coherent QDs in sample *A* have a lower lattice mismatch (i.e., a lower In composition) than in sample *B* (the question of whether there might also be different indium compositions in incoherent islands and coherent QDs, because of their different ripening behavior [13], cannot be assessed from this data).

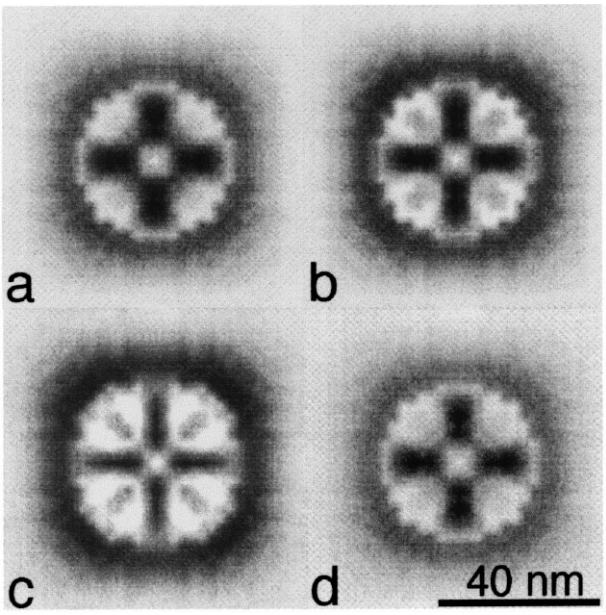

FIG. 4. Simulated images for model QDs with a base diameter 40 nm, an aspect ratio of height to base diameter 1:4, and lattice mismatches (a) 4%, (b) 6%, (c) 7%, and (d) with the lattice mismatch varying from 4% at the bottom to 6% at the top. The following imaging conditions are used: sample thickness, 70 nm, which is defined as the thickness from the film bottom to the top of the QD; electron accelerating voltage, 120 kV; number of diffracted beams included in the calculation, 29.

The bar in Fig. 2 is not of constant width [as it is in the simulated images Figs. 4(a)–4(c)], but appears as a trapezoid or a triangle. To explain this difference, it is noted that, in the above simulated images, the chemical composition in the QD was assumed to be constant throughout the QD, so that a constant lattice mismatch was used in each case. However, indium segregation to the growing surface, which results in indium surface enrichment, is a common phenomenon in the $In_xGa_{1-x}As/GaAs$ quantum well system [14,15]. Elemental segregation has also been reported in InGaAs/GaAs [3] and GeSi/Si QD system [16]. For this reason, images were simulated for QDs with chemical composition varying through the QDs. This was done by varying the lattice mismatch in the

different layers of a QD. Based on the facts that (i) as shown in Figures 4(a)–4(c), the width of the bars becomes narrower with increasing the lattice mismatch and (ii) lattice mismatch has been reported to increase from the bottom towards the top of the QD [3,16], the lattice mismatch was varied from $f = 4\%$ at the bottom of the QD to $f = 6\%$ at the top. Figure 4(d) shows the resulting simulated image. It is seen that the width of the cross bars is no longer a constant. This result is in good agreement with the experimental image and is consistent with there being indium segregation in the QDs. To this point, it has not been possible to take into account any contrast effects caused by the variation in structure factor due to the segregation (so-called "structure factor contrast"). Preliminary simulations suggest that the effect is small, but a further study is necessary.

We have investigated images for several other different segregation models (including the model of Tersoff [9] in which the indium concentration is high at the core of the QD). In all cases where the indium concentration is high towards the symmetry axis of the QD, and low near the region A in Fig. 3, the bars of the image are triangular in shape and different from the parallel bars where the QD has uniform indium concentration. To this point, we are unable to differentiate between the several segregation models using the images, except to say that models with segregation agree with the experimental images, while models without segregation do not agree. Further experiments are needed to investigate the direction of indium segregation.

Differences in contrast with size need to be established by simulation, but our preliminary results show that the larger islands exhibit stronger segregation and weaker enrichment, since detailed examination of images such as those shown in Figs. 2(a) and 2(b) reveals that the bars in the images of sample *A* are more triangular than those of sample *B*. This might be due to a difference in the extent of segregation in the two samples and this is being further investigated. Since high temperature growth also achieves lower island concentration, effects on segregation could be expected since formation of larger islands in lower densities might impact the kinetics of island growth [9].

Island stability is a key issue in technological application of quantum dots. The possibility of stable islands has been demonstrated theoretically [17]. Stable nonripening islands have also been demonstrated experimentally for optimum values of AsH_3 partial pressure in similar metal-organic chemical-vapor deposition grown dots [8]. Indium segregation in stable and metastable islands needs to be investigated further (as well as indium redistribution before and after annealing) to determine if there is a link between segregation and island metastability.

In summary, image simulations of [001] on-zone bright-field images of $In_xGa_{1-x}As$ QDs on (001) GaAs, based on strain field distributions obtained from finite element analysis, have been used to study the size, mismatch, and composition distribution in QDs. In particular, the study shows indium enrichment and segregation in the coherently strained InGaAs QDs.

We thank the Australian Research Council for providing financial support and the Sydney Regional Visualisation Laboratory for facilities for the calculation of the strain distribution. R. Leon would like to thank the Jet Propulsion Laboratory for financial support. Professor S. Matsumura, Dr. G. Anstis, and Dr. C. Goringe are thanked for their assistance with programming.

[1] R. Leon *et al.*, Appl. Phys. Lett. **67**, 521 (1995); H. Jiang and J. Singh, Phys. Rev. B **56**, 4696 (1997); J. L. Zhu *et al.*, Phys. Rev. B **55**, 15 819 (1997).
[2] See, for example, X. Z. Liao *et al.*, Phys. Rev. B **58**, R4235 (1998), and references therein.
[3] A. Rosenauer *et al.*, Appl. Phys. Lett. **71**, 3868 (1997).
[4] S. Christiansen *et al.*, Appl. Phys. Lett. **64**, 3617 (1994).
[5] T. Benabbas *et al.*, J. Appl. Phys. **80**, 2763 (1996).
[6] J. Zou *et al.*, Phys. Rev. B **59**, 12 279 (1999).
[7] R. Leon *et al.*, Appl. Phys. Lett. **69**, 1888 (1996); R. Leon *et al.*, Phys. Rev. Lett. **78**, 4942 (1997).
[8] R. Leon *et al.*, Phys. Rev. Lett. **81**, 2486 (1998).
[9] J. Tersoff, Phys. Rev. Lett. **81**, 3183 (1998).
[10] http://www.strand.com.au
[11] J. S. Blakemore, J. Appl. Phys. **53**, R123 (1982).
[12] C. J. Humphreys, Rep. Prog. Phys. **42**, 1825 (1979).
[13] J. Drucker, Phys. Rev. B **48**, 18 203 (1993).
[14] O. Dehaese, X. Wallart, and F. Mollot, Appl. Phys. Lett. **66**, 52 (1995).
[15] J. P. McCaffrey *et al.*, Philos. Mag. A **75**, 803 (1997).
[16] T. Walther, C. J. Humphreys, and A. G. Cullis, Appl. Phys. Lett. **71**, 809 (1997).
[17] V. A. Shchukin *et al.*, Phys. Rev. Lett. **75**, 2968 (1995); I. Daruka and A.-L. Barabasi, Phys. Rev. Lett. **79**, 3708 (1997); Appl. Phys. Lett. **72**, 2102 (1998).